JOURNAL OF COMPUTATIONAL PHYSICS 69, 325–340 (1987)

A Non-self-adjoint General Matrix Eigenvalue Problem

G. DELIC, E. J. JANSE VAN RENSBURG, AND G. WELKE

Nuclear Theory Research Group, Department of Physics, and Schonland Research Center for Nuclear Sciences, University of the Witwatersrand, 1 Jan Smuts Avenue, Johannesburg 2001, South Africa

Received February 27, 1985; revised May 2, 1986

A Chebyshev polynomial method proposed previously was used to study the spectral properties of a non-self-adjoint Sturmian eigenvalue equation encountered in Quantum Scattering theory. A study of numerical convergence behaviour showed that improved convergence occurs for solutions corresponding to potentials which change sign in the interval of approximation. Continuous variation of such nodal potentials leads to migration of eigenvalues in the complex eigenvalue plane and to growth of new branches in the spectrum. A numerical stability study evaluated the performance of three commonly available subroutine paths for the complex general matrix eigenvalue problem which results in the present method. © 1987 Academic Press, Inc.

I. INTRODUCTION

The spectral theory of self-adjoint operators has developed through the use of ideas centered on the theory of linear operators in Hilbert space [1]. The importance of self-adjoint operators is due to engineering and scientific applications where the spectrum is on the real line [2]. However, investigations in Quantum Scattering theory [3], Transport theory [4] and Hydrodynamics [5] lead to the study of differential and integral operators which are not self-adjoint. The spectral theory of non-self-adjoint operators is still a relatively young subject [6] when compared to the self-adjoint case [7]. Recently mathematical treatises on the theory of non-self-adjoint operators have appeared [8, 9].

Numerical studies of algorithms for non-self-adjoint operator equations are important from the point of view of applications because they establish stability (or lack of it) of discrete approximations to such equations. In a previous communication [10] a non-self-adjoint second order differential equation, which arises in Quantum Scattering theory [11], was solved by introducing a set of polynomial functions spanning a Hilbert space defined by an inner product with the Chebyshev weight. Approximations to the solutions of the differential equation with such a Chebyshev set (on a finite interval) is expected to show convergence. This is because the polynomials with complex rational coefficients are dense in the space of functions solving the differential equation. The method of [10] showed satisfactory convergence for both eigenvalues and eigenfunctions, but substantial improvements

0021-9991/87 $3.00

in efficiency are possible. Also, the previous work studied only the case of potentials of constant sign, whereas realistic physical models [12] have potentials which oscillate in the interval of approximation. For this reason the present study has investigated further the convergence properties of the Chebyshev set and the R algorithm of [10]. In the course of the investigation important discoveries were made relating to the spectral properties of the non-self-adjoint Sturmian eigenvalue equation. Improved convergence was found for solutions corresponding to potentials which change sign in the interval of approximation. Continuous variation of such nodal potentials leads to migration of eigenvalues in the complex eigenvalue plane and to growth of new branches in the spectrum. The method of [10] leads to a complex general matrix eigenvalue problem and a recent survey [13] found "very little in the way of proven techniques" for such cases. This situation and also some serious numerical problems in the present work suggested the comparison of numerical stability in different subroutine packages.

Section II discusses the method, Section III describes the eigenvalue spectrum, Section IV investigates the L_2 error for the eigenfunctions, Section V discusses the question of numerical stability and Section VI summarises the conclusions.

II. Method

In operator form the equation to be solved is

$$Av = \alpha \bar{V} v \tag{1}$$

and is described in detail in Section II of [10]. In Eq. (1), A is a second order differential operator with terms containing a complex potential V_0 and the usual term in $l(l+1)/r^2$, where l is the (integer) orbital angular momentum. In Quantum Scattering theory applications [11] the boundary conditions are that the solution is regular at the origin and has "outgoing waves" asymptotically as discussed in Appendix A of [10]. For this choice of boundary conditions Eq. (1) is a Sturmian eigenvalue equation and the solutions form a discrete sequence of complex functions $v_{lj}(r)$ ordered strictly according to increasing magnitude of the complex eigenvalues α_{lj}, $j = 1, 2, 3, \ldots$, for each l. The complex potentials $V_0(r)$ and $\bar{V}(r)$ are considered to be negligibly small at some radius $r = a$, where, for all j, the $v_{lj}(a)$ satisfy the boundary condition Eq. (A3) of [10] and are normalized according to Eq. (29) of that reference. A short history of the occurence of Eq. (1) in Nuclear Quantum Scattering Theory is to be found in [14]. It appears that in nuclear physics there has so far been no investigation of the case that either of the complex bounded potential functions of Eq. (1) oscillates in the interval of approximation.

In the method of [10] the solution $v_{lj}(r)$ is expanded in a series of even Chebyshev polynomials on the interval $r \in [0, a]$

$$v_{lj}(r) = \pi^{1/2}(r/2)^{l+1} \sum_{n=0}^{\infty}{}' b_n^{lj}(a)\, T_{2n}(x) \tag{2}$$

with the prime indicating that the first term has the factor $\frac{1}{2}$ and where $r = ax$, $x \in [-1, +1]$. The solution v_{lj} is approximated by truncating the summation of Eq. (2) at some $n = N_m$. Application of the boundary condition at $r = a$ shows that only coefficients for $n = 1$ to N_m are linearly independent. The latter are then solution vectors of a complex general matrix eigenvalue problem of the form

$$\mathbf{R}\mathbf{b}^l = \alpha_l \mathbf{H}\mathbf{b}^l \tag{3}$$

as described in Section III of [10].

Applications where both **R** and **H** are real symmetric [15] or real banded [16] matrices are not uncommon. But in the present work both matrices **R** and **H** are complex and non-Hermitian while only **H** is symmetric. In [10] Eq. (3) was solved by Algorithm *R*, which assumes the existence of a Cholesky decomposition for **H**. The present work investigated the convergence behaviour of the *R* algorithm as $\bar{V}$ in Eq. (1) was varied in a range typical of realistic physical potentials. Variation of $\bar{V}$ reveals differing numerical convergence properties of the *R* Algorithm and even loss of numerical stability in some eigenvalue–eigenvector subroutines. Therefore three different numerical methods of solving the complex general eigenvalue problem are compared in Section V.

A deficiency of the method in [10] is that the Chebyshev expansion coefficients of V_0 and $\bar{V}$ must be computed by quadrature. An alternative approach is to choose analytical forms for which the Chebyshev expansion coefficients are either known in closed form or may be computed by recurrence. An appropriate choice is the form

$$Ve^{-\gamma^2 r^2}(c_0 + c_1 r^2 + c_2 r^4) \tag{4}$$

with $r = ax$. Following Luke [17], the Chebyshev expansion of $N_v + 1$ terms for the Gaussian factor is

$$e^{-\gamma^2 r^2} = e^{-\gamma^2 a^2} \sum_{n=0}^{N_v}{}' (-1)^n E_n(\gamma^2 a^2)\, T_{2n}(x). \tag{5}$$

The coefficient E_n satisfies the four term recurrence (pp. 35, 313–314 of [17]):

$$\begin{aligned}\{n/(n+1)\}\, E_n = &\{-(n+3)/(n+2) + 4n/(\gamma^4 a^4)\}\, E_{n+1} \\ &+ \{n/(n+1) + 4(n+3)/(\gamma^4 a^4)\}\, E_{n+2} \\ &+ \{(n+3)/(n+2)\}\, E_{n+3}.\end{aligned} \tag{6}$$

The constants in Eq. (4) may be adjusted to give potentials approximating closely Woods–Saxon forms of the type discussed in [10] with the numerical advantage that the potentials $V_0(r)$ and $\bar{V}(r)$ will approximate zero very closely at a suitable truncation radius $r = a$. The important advantages of the recurrence (6) are that the coefficients are generated with a high degree of precision and that they decrease very rapidly in magnitude as n increases. Typically, with 35 terms in the Chebyshev expansion for (4) accuracy of 16 significant figures is obtained on an interval

$r \in [0, 8.38\ \text{fm}]$ for the choice of parameters discussed here. The importance of the substantially improved accuracy in a recurrence method is that it makes for easier detection of accumulation errors in eigenvalue–eigenvector subroutine packages.

A useful feature of potentials of the form (4) is that a node may be introduced at some $r_0 \in [0, a]$. Since oscillatory potentials are typical of case studies from Nuclear Quantum Scattering [12] such potentials have been studied systematically in the present work. The parameters used in Eq. (4) for those cases discussed in Sections III and IV are summarised in Table I.

III. The Eigenvalue Spectrum

The eigenvalue spectrum of Eq. (1) was computed by the R-Algorithm of [10] for cases P1 to P3 and Q1 to Q12 of Table I. All calculations reported here used the

TABLE I

Potential Parameters for Cases P1 to P3 and Q1 to Q12[a]

		Real part					Imaginary part[b]			
Case[c]		Node (fm)	V (MeV)	γ (fm^{-1})	c_0	c_1 (fm^{-2})	c_2 (fm^{-4})	V (MeV)	γ (fm^{-1})	c_2 (fm^{-4})
$P1$	V_0	none	−52.5	0.46106	0.48	0.14	0.0	−0.53552	0.4909	1.0
	$\bar{V}$	none	−52.5	0.46106	0.48	0.14	0.0	−0.53552	0.4909	1.0
$P2$	V_0	none	−52.5	0.46106	0.48	0.14	0.0	−0.53552	0.4909	1.0
	$\bar{V}$	2.50	−83.3	0.445	0.3	−0.04783	0.0	0.0	1.0	0.0
$P3$	V_0	2.50	−83.3	0.445	0.3	−0.04783	0.0	−0.86337	0.55292	1.0
	$\bar{V}$	none	−0.53552	0.4909	0.0	0.0	1.0	−0.53552	0.4909	1.0
$Q1$	V_0	none	−50.0	0.49754	0.5	0.15	0.0			
	$\bar{V}$	5.79	−83.3	0.39	0.3	−0.00894	0.0			
$Q2$		5.27		0.40		−0.01080				
$Q3$		4.67		0.41		−0.01375				
$Q4$		4.03		0.42		−0.01849				
$Q5$		3.70		0.425		−0.02187				
$Q6$		3.39		0.430		−0.02617				
$Q7$		3.08		0.435		−0.03168				
$Q8$		2.78		0.440		−0.03875				
$Q9$		2.50		0.445		−0.04783				
$Q10$		2.24		0.450		−0.05956				
$Q11$		2.00		0.455		−0.07472				
$Q12$		1.78		0.460		−0.09436				

[a] The form of the real (or imaginary) part of the potential is $Ve^{-\gamma^2 r^2}(c_0 + c_1 r^2 + c_2 r^4)$.

[b] In all cases $c_0 = c_1 = 0$ with no node.

[c] Cases Q1 to Q12 all have the same V_0 and no imaginary term is included for either V_0 or $\bar{V}$. The location of the node is given in units of fm in parentheses.

kinematical parameters of [10]. These correspond to the quantum mechanical description of a 15 million electron volt (MeV) neutron scattering from ^{16}O in the laboratory coordinate system. In Eqs. (4) to (6) of [10], values of the constants used were: wave number $k = 0.7972152$ fm^{-1}, center-of-mass energy $E = 14.11$ MeV and $2\mu/\hbar^2 = 0.045018$ fm^{-2} MeV^{-1}. The truncation radius was $a = 8.38$ fm and the abbreviation fm denotes the nuclear physics unit of length, namely, the Fermi.

Case P1 was chosen to closely reproduce the shape of case five from [10] near the point of inflection of the real part of V_0. The resulting real part of P1 was approximately 2 MeV deeper than the Woods–Saxon form at $r = 1$ and 4 fm. The corresponding imaginary part was slightly broader than the Woods–Saxon derivative form of case five [10]. In view of this choice of potential parameters the eigenvalue spectrum of P1 is very similar to that of case five of [10] and the convergence properties are also similar, as will now be discussed. Convergence behaviour as a function of matrix size was measured by plotting the magnitude of each eigenvalue as a function of the matrix order required for convergence to four significant figures. Such a plot is important in assessing how large a matrix is required to ensure convergence of all complex eigenvalues lying inside a circle of prescribed radius in the Argand plane. The points in this plot tend to cluster along a line and convergence is measured by the slope of the line. In Fig. 4 of [10] for case five, and also P1 in the present work, this slope is 2.7.

Potentials of the type P1, or case five of [10] (see Fig. 5 of that reference), all have eigenvalue spectra consisting of one branch extending away from the origin into the fourth quadrant of the complex eigenvalue plane. However, the character of the spectrum changes if $\bar{V}$ has a node, and consequently changes sign, inside the range of V_0, which is a situation typical of some realistic physical cases [12]. An example is case P2, where V_0 is the same as used in P1, but $\bar{V}$ has a node at $r_0 = 2.5$ fm. The eigenvalue spectrum of P2 is shown in Fig. 1a, where a second branch of the spectrum is evident in the second quadrant. Fig. 1a also shows the spectrum of case P3, where the node is in V_0 and not in $\bar{V}$. Case P3 has only one branch in its eigenvalue spectrum, but real and imaginary parts have a similar magnitude and therefore the descent into the complex plane is much steeper than for cases P1 or P2.

The evolution of the second branch in the spectrum for cases similar to P2 was studied by systematic variation of $\bar{V}$. Table I gives parameters and node location for the cases Q1 to Q12 which all have a fixed potential V_0 similar in shape to V_0 of P1, but displaced by ~ 0.3 fm towards smaller radii. The evolution of a second branch in the spectrum is shown in Fig. 1b, where initially (for Q3) there is only one branch in the spectrum in this region of the Argand plane. As the node r_0 in the potential $\bar{V}$ moves towards smaller radii, the volume of $\bar{V}$ in the interval $r \in [0, r_0]$, where $\bar{V}(r) < 0$, decreases and the distance between successive eigenvalues on the first branch correspondingly increases. Thus Q12 has approximately half the number of eigenvalues remaining on this branch compared to Q3. When $r_0 = 4.03$ fm for Q4 an eigenvalue has appeared in the first quadrant far from the origin and moves closer to the origin as r_0 decreases. Similarly, other eigenvalues appear in the

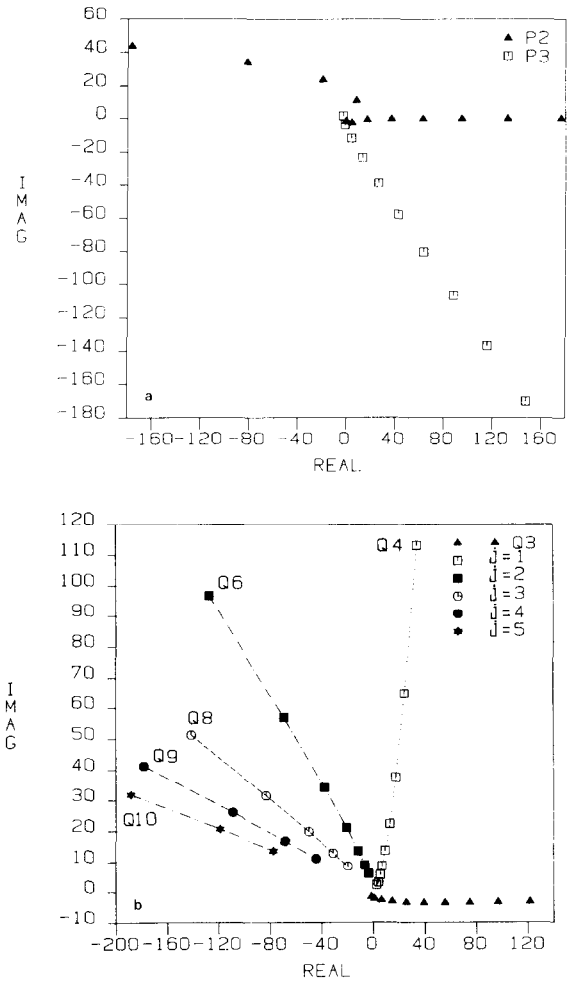

FIG. 1. (a) Argand plot of eigenvalues for cases P2 and P3 of Table I with $l=0$. Case P2 has a second branch in the spectrum whereas P3 does not. The eigenvalue spectrum of case Q9, where neither V_0 nor $\bar{V}$ has an imaginary potential, differs only slightly from that of case P2 shown here. (b) Argand plot of eigenvalues for cases Q3 to Q12 of Table I with $l=0$. The spectrum of Q3 is shown by the opaque triangles. For the cases Q4 to Q12 the branch for which $\mathrm{Re}(\alpha)$ is positive lies on the same curve as that for case Q3 with a small but non-zero value for $\mathrm{Im}(\alpha)$. However, the separation between eigenvalues on this branch increases from case Q3 to Q12 as described in the text. The other symbols show eigenvalues on the second branch of the spectrum in the first and second quadrants. Their hierarchy on this branch is labelled by j in the symbol key. The points furthest from the origin on each curve are labelled by the case for which that eigenvalue first appears. Each curve shows the trajectory of an eigenvalue as $\bar{V}$ approaches Q12 in the increments listed in Table I. The first five eigenvalues of the second branch of the spectrum for Q12 are the trajectory end points closest to the origin.

second quadrant as shown in Fig. 1b, and approach the real axis from large distances as r_0 decreases. Thus, case Q12 has two distinct branches in the eigenvalue spectrum and each contains a similar number of eigenvalues. Such results are also found for $l = 4$, 6 and 8, but are not shown here.

The growth of the second branch of the spectrum corresponds to the increase in volume of $\bar{V}$ in the interval $r \in [r_0, a]$, where $\bar{V}(r) > 0$. This behaviour for the non-self-adjoint problem of the present study is the analogue of the simpler example of [18]. In the latter case negative and positive branches of real eigenvalues are present if the weight function $\bar{V}$ is indefinite and has nodes or "turning points" (see [19] for papers by F. V. Atkinson and D. Jabon, B. Ćurgus and H. Langer, J. Fleckinger and H. El Fetnassi, M. L. Lapidus, and H. D. Niessen). The effect of the non-self-adjoint boundary condition is to rotate the respective branches into the complex eigenvalue plane away from the real line. An interesting interpretation has been proposed by Kaper *et al.* [20–22], who made case studies of some simple examples. These authors proposed [21] that eigenfunctions corresponding to eigenvalues on the respective branches of the spectrum form two separate bases of the two Hilbert spaces of functions defined on the two intervals divided by the node in $\bar{V}$. This proposal and its consequences are discussed further in Chapter 4 of [4] and are also the subject of further study in an application to the Quantum Scattering case [23].

A referee of the present work has suggested a simple argument which develops an understanding of how two spectral branches are possible. For case P2 of Table I the first eight eigenvalues are given in Table II. Since $\bar{V}$ has no imaginary part, the potential sum $V_0 + \alpha_{lj}\bar{V}$ has a real part which is negative at the origin if α_{lj} has a positive real part. This is the case for eigenvalues $j = 2$, 3, 4, 6, 7 and this potential sum also has a real part which is positive for $r \geqslant r_0$. This positive barrier region determines the character of the eigenfunction. If the barrier has a height which is less than the energy of the scattered wave, as is the case for $j = 2$, then the eigenfunction is oscillatory for all r. However, if the barrier height is greater than the

TABLE II

Eigenvalues for Case P2[a]

j	N_m	Real	Imaginary	Magnitude
1	28	−0.696160	−1.999404	2.117134
2	32	4.306277	−2.858216	5.168503
3	40	8.066303	10.701471	13.400997
4	42	16.826706	−1.018691	16.857513
5	42	−19.532981	23.686633	30.701693
6	50	37.011024	−0.502557	37.014436
7	58	62.892853	−0.425780	62.894295
8	48	−81.657069	33.884346	88.408290

[a] The second column shows the matrix size required for each eigenvalue to produce convergence to the number of significant figures tabulated.

incident energy, which is the case for $j \geq 4$, then the eigenfunction is monotonic in the barrier region $r > r_0$ and oscillatory for $r < r_0$. A typical example of this behaviour is shown in Fig. 2a for $j = 6$. The converse case corresponds to the second branch of the spectrum, where α_{lj} has a real part which is negative and the potential sum has a resultant real part which is positive at the origin. This is the case for eigenvalues $j = 5$ and 8 while for $j = 1$ the real part of the potential sum is not yet positive. Since eigenvalues increase rapidly in magnitude the real part of the potential sum also increases in the region $r < r_0$ but still approaches zero as r approaches r_0 and then becomes negative when $r > r_0$. Consequently, the eigenfunction tends to be small or monotonic for $r < r_0$ and oscillatory for $r > r_0$. The example of $j = 5$ is shown in Fig. 2b. The results of Fig. 2 are typical of the larger eigenvalues and give a clear indication of how two separate bases arise corresponding to the two regions of r on either side of r_0. The above argument can be expanded to include the consequences of the oscillatory imaginary part of the potential sum.

In studying the evolution of the spectrum for cases Q1 to Q12 it was noted that enhanced numerical convergence occurred for $l = 0, 4, 6$ and 8 when $2 \leqslant r_0 \leqslant 3$ fm,

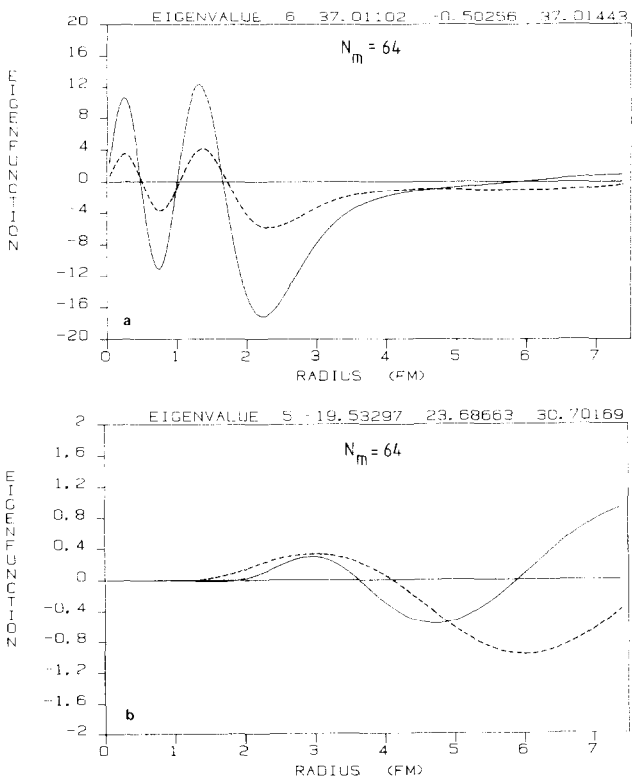

FIG. 2. Eigenfunctions of case P2 with $l = 0$ corresponding to (a) $j = 6$ and (b) $j = 5$ for a matrix size $N_m = 64$. The real part is the unbroken line and the imaginary part is the dashed line. Also shown on the top of each frame are real and imaginary parts of the eigenvalue as well as the magnitude.

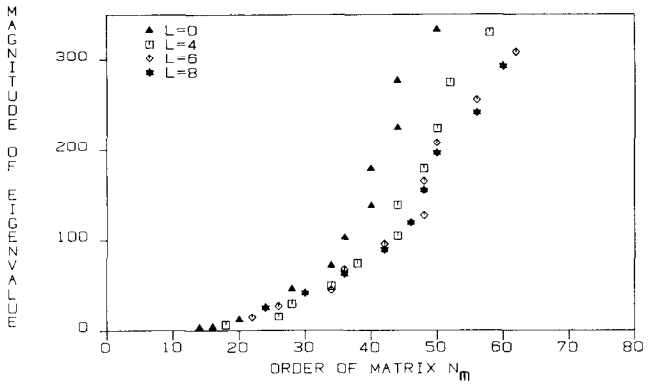

FIG. 3. Magnitude of eigenvalues for $l = 0, 4, 6$ and 8 as a function of the matrix order N_m required to produce convergence to four significant figures for case P3 of Table I.

namely, cases Q7 to Q11. The enhanced convergence consisted of eigenvalues of magnitude up to 200 being computed correctly to four significant figures for matrix sizes $\leqslant 60$. This is in contrast to the convergence behaviour of cases such as P1 discussed above. This improvement in convergence is a consequence of the right-hand side of Eq. (1) vanishing when $\bar{V} = 0$ at the node r_0. This imposes a constraint on the matrix, namely $Av = 0$, which all eigenvectors must satisfy at the node, in addition to the two boundary conditions. This constraint is present only when the node in $\bar{V}$ is present and leads to significant gains in convergence when this node is in the vicinity of the point of inflection of V_0.

For case P3, Fig. 3 shows a plot of the magnitude of the eigenvalues against the matrix order required to produce convergence to four significant figures. The initial slope for $N_m \leqslant 40$ is 4 and increases sharply to 15 for $N_m \geqslant 40$. This result is substantially better than the 2.7 obtained for cases such as P1, discussed above. Therefore the result shown in Fig. 3 for case P3 represents an improvement in convergence of the eigenvalues by a factor of two to five over the results obtained for cases like P1.

IV. L_2 Error for Eigenfunctions

If $u_{lj}(r)$ is the sum to infinity in the right-hand side of Eq. (2) and $u_{lj}^{(N)}(r)$ is the sum to N terms, then the L_2 error is defined as the norm of $u_{lj}(r) - u_{lj}^{(N)}(r)$ in the N-dimensional Hilbert space with the inner product defined in Eq. (22) of [10]. Thus

$$L_2^{lj}(a)_N = \|u_{lj} - u_{lj}^{(N)}\| = \sqrt{\left\{\frac{1}{2}\pi \sum_{n=N+1}^{\infty} [b_n^{lj}(a)]^2\right\}} \tag{7}$$

which follows from the properties of Chebyshev polynomials. It is implicit in the truncation of the summation in Eq. (7) at $n = N_m$ that the coefficients obtained from

the R algorithm of rank N_m are the exact Chebyshev coefficients. In view of the results of [10] this is the case if N_m is sufficiently large. In the present application the coefficients b_n^{lj} are complex numbers and therefore the number defining L_2 is complex. However, since only magnitudes are significant in measuring error, the L_2 error is taken as the square root of the modulus of the term in cusped parentheses. This procedure obviates the need for showing both real and imaginary parts of the L_2 error separately.

The L_2 error is a concise measure of the error remaining on truncation of the summation after N terms. It provides a more convenient measure of the error than does inspection of the error curve as was done previously [10]. However, the L_2 error as defined in (7) does not contain the r^{l+1} term of Eq. (2). Therefore, the same magnitude for $L_2^{lj}(a)_N$ for differing l could imply a deterioration in the error curve for increasing l, but for fixed l a comparison of L_2 errors in meaningful.

It will now be shown that the L_2 error is not directly correlated with the number of nodes in the wave function. This is illustrated in Fig. 4, which compares the L_2

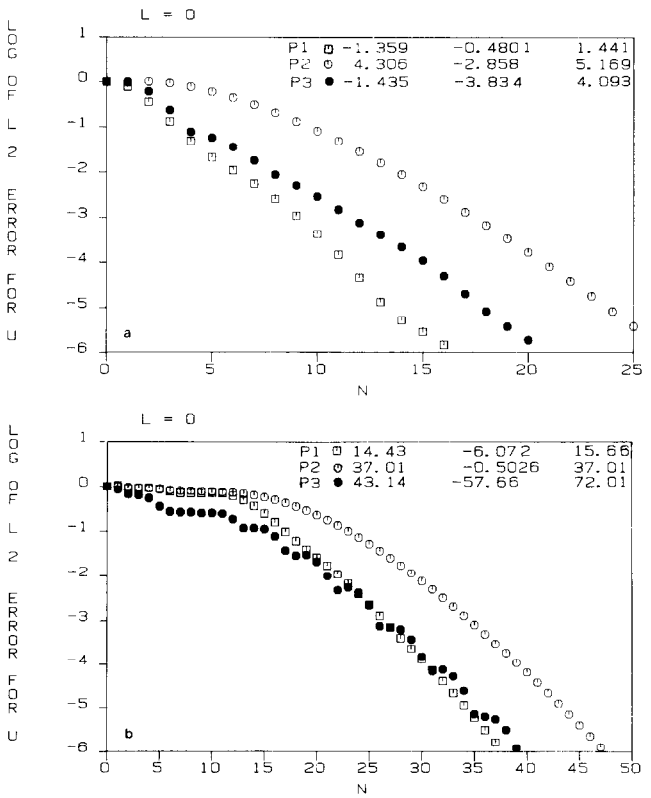

FIG. 4. (a) The log of the L_2 error of Eq. (7) (normalised to zero) for the eigenfunction corresponding to eigenvalue $j=2$ with $l=0$ for cases P1 (squares), P2 (open circles) and P3 (opaque circles). The symbol key gives real and imaginary parts of the eigenvalue as well as the magnitude. (b) As in (a) for $j=6$ with $l=0$. Note the change in scale in the abscissa.

error for $l=0$, $j=2$ (part a) and $j=6$ (part b) for three different cases, P1, P2 and P3. The larger the value of j, the larger is the number of nodes in the wavefunction and also the magnitude of the eigenvalue. The three cases are normalised to zero at $N=0$ and in each case the error decreases rapidly. It is expected that eigenvalues of larger magnitude require more terms in Eq. (2) to produce the same error in the eigenfunction as do eigenvalues of smaller magnitude. This is due to the fact that, in general, larger eigenvalues correspond to eigenfunctions which have more oscillations inside the range of V_0 compared to eigenfunctions of smaller eigenvalues [10]. Figure 4b shows the L_2 errors of $l=0$, $j=6$ corresponding to the same cases as those of Fig. 4a for $j=2$. The ratio of magnitudes of the eigenvalues $j=6$ and 2 is $\geqslant 10$, but the N value required for the same L_2 error $\sim 10^{-5}$ only doubles. In Fig. 4b, a comparison of cases P1, P2 and P3 shows that while the magnitude of the eigenvalue for $j=6$ approximately doubles from one case to the next, the size of N for the same L_2 error increases slightly for P2 and is the same for P3. Therefore, for fixed N, a prescribed L_2 error in the eigenfunctions is maintained in case P3 for complex eigenvalues of much larger modulus compared to case P1.

V. Numerical Stability

In this section the L_2 error will be examined as a function of the size N_m of the matrix to be diagonalized. Since N_m is the upper limit in the sum of Eq. (7) N runs from 1 to N_m. One would expect that the L_2 error does not depend on N_m unless N is close to N_m. This is indeed the case as is shown in parts (a) and (b) of Fig. 5. However, for $N_m=54$, one of the three diagonalization routines used fails to reduce the L_2 error as N is increased, as is shown in Fig. 5c.

In the variation of $\bar{V}$ described in Section III it was found that the first two eigenvalues can have the same magnitude and thereby differ only in phase. This situation resulted in reduced accuracy in the R-algorithm of [10] and is thus a suitable case for investigation of stability in eigenvalue–eigenvector software. For this investigation the potential V_0 was that used in cases Q1 to Q12 of Table I while $\bar{V}$ was chosen such that the magnitudes of eigenvalues $j=1$ and $j=2$ agreed to eight significant figures. The corresponding parameters of the real part of $\bar{V}$ were $V=83.\overline{3}$ MeV, $\gamma=0.4082$ fm^{-1}, $c_0=0.3$, $c_1=-0.013491547$ fm^{-2}, $c_2=0$ fm^{-4}, with no imaginary part. The eigenfunctions generated from the eigenvectors for $j=1$ and $j=2$, while similar, are linearly independent, since they differ in the occurrence of an additional node in the imaginary part.

Three different diagonalisation routines were then used to investigate for this case the L_2 error of the first six eigenvectors and the convergence of the corresponding eigenvalues as a function of the matrix order in Eq. (3). The matrix diagonalisations of Algorithm R [10] were performed using the Matrix Eigensystem Routines of EISPACK [24]. This package offers two ways in which eigenvalues and eigenvectors of a complex general matrix may be computed. The first path (subroutines CBAL, COMHES, COMLR2 and CBABK2), referred to here as the LR path, uses

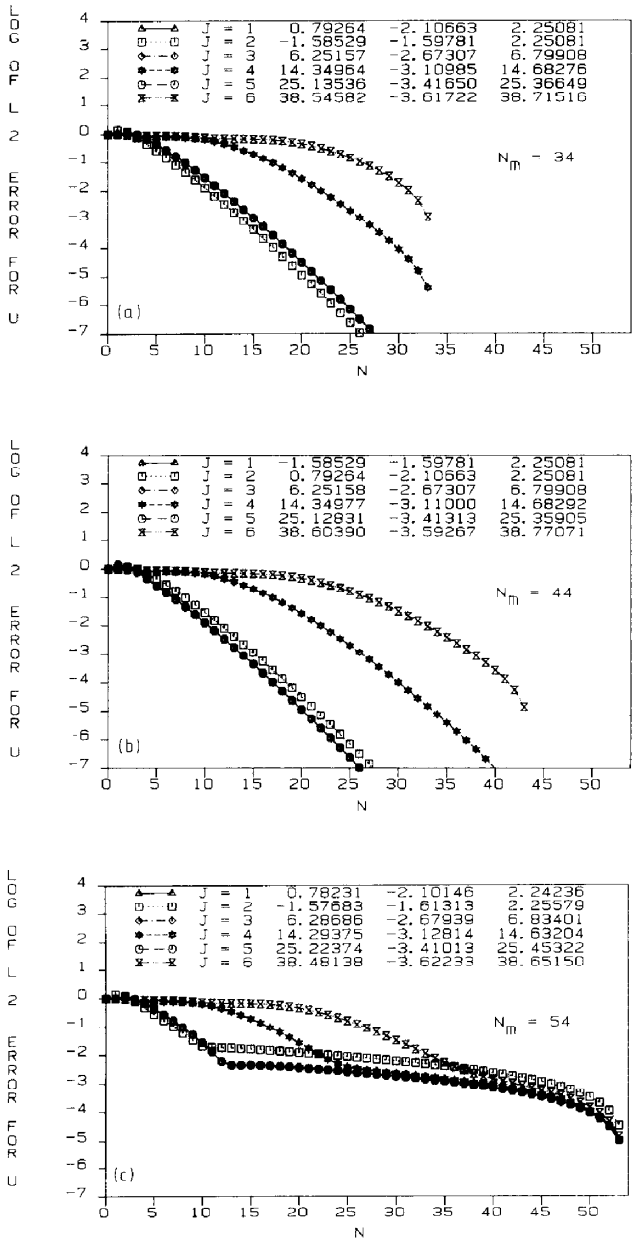

FIG. 5. Log of the L_2 error of Eq. (7) for eigenfunctions $j = 1$ to 6 with the choice of potential parameters given in Section V. The symbol key gives real and imaginary parts of each eigenvalue and the magnitude. The matrix order in the diagonalisation of Eq. (3) is given by N_m. The results of the LR path correspond to (a), (b) and (c) while (d) is for the QZ path. Note that the L_2 errors for $j = 1$, 3 and 5 are superposed.

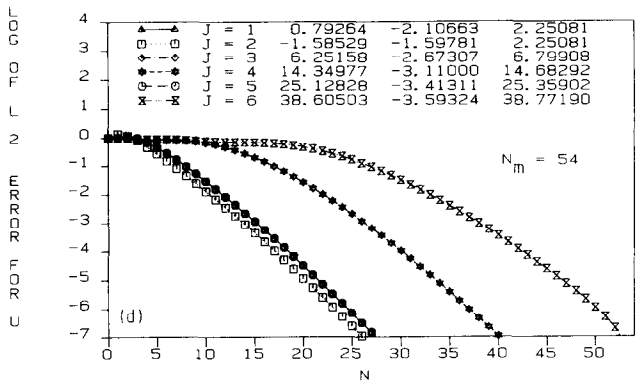

FIG. 5—*Continued.*

stabilised elementary similarity transformations. The second path (subroutines CBAL, CORTH, COMQR2, CBABK2), referred to here as the QR path, uses unitary similarity transformations. The third routine used was the QZ path of Moler and Stewart [25]. While both the LR and the QR paths require the R-algorithm of [10] the QZ path does not since it diagonalises matrices **R** and **H** simultaneously. The QZ path is available in two versions: one is part of the IMSL subroutine package [26] (subroutines EIGZC, ELZHC, ELZVC, UERTST, UGETIO) and the other is part of the NAGLIB package [27] (subroutines A02AAF, A02ABF, A02ACF, F02GJF, F02GJX, F02GJY, F02GJZ, P01AAF, X02AAF). The calculations reported here used the former, but a comparison with the latter was also made.

Figure 5a shows the L_2 error of Eq. (7) as a function of N, where, however, the $b_n^{lj}(a)$ result from the diagonalisation of a matrix of dimension $N_m = 34$. Figure 5b corresponds to the case $N_m = 44$. The L_2 errors of all the odd-numbered eigenvectors (which are numbered according to increasing eigenvalue magnitude) are superposed. For the even-numbered eigenvectors, the larger the magnitude of the corresponding eigenvalue, the larger the matrix size required to obtain a prescribed value of the L_2 error. Accuracy is limited to $\log_{10}(L_2) \geqslant -7$ because the choice of Sommerfeld parameter (see Section IV of Ref. [10]) results in an error in the boundary condition of order 10^{-7}. The LR path fails to reduce the L_2 error as N is increased for N_m above approximately 50. The failure is due to error propagation in the LR path and is particularly acute for $N_m = 54$ as is shown in Fig. 5c. This problem was not observed (to within the boundary condition error) in either the QR or QZ path. The results of the latter paths for $N_m = 54$ are shown in Fig. 5d.

Apart from the L_2 error, another method of measuring numerical accuracy in eigenvectors for a fixed N_m, and also stability as N_m increases, is by inspection of the sum

$$u_{lj}^{(N)}(r) = \sum_{n=0}^{N}{}' \, b_n^{lj}(a) \, T_{2n}(x) \tag{8}$$

(for $N = N_m$) at the origin ($x = 0$) and the truncation radius ($x = 1$). In such a comparison the IMSL and NAGLIB versions of the QZ path gave similar accuracy for fixed N_m, but the NAGLIB path was more stable against increasing N_m. In comparing different routines typical results were that for the first few eigenvectors the LR, QZ and QR paths gave, respectively, 5, 6 and 7 (often 8) significant figures. Similarly, in the calculation of eigenvalues, the same trend occurred and the corresponding significant figures were 6, 7 and ~ 8, respectively. This indicates that error propagation is most prominent in the LR path and least prominent in the QR path.

The total CPU time used to solve the complex general matrix eigenvalue problem of Eq. (3) was compared for the three different paths. On an IBM 3083E8 processor with double precision arithmetic using the IBM FORTRAN VS (Version 2.0) compiler, an equation of the form

$$t\,(\text{sec}) = \alpha N_m^{\beta} \tag{9}$$

gave good fits to the data for computation times with N_m in the range 20 to 80. The values of α and β found were, respectively, 1.0×10^{-5} and 3.9 for the LR path; 2.2×10^{-5} and 3.7 for the QR path; and 4.3×10^{-5} and 3.0 for the QZ (IMSL) path. For matrix sizes $N_m > 80$ the IMSL QZ implementation failed. However, the NAGLIB QZ routine did not fail for $N_m \leqslant 120$ and the timing runs yielded $\alpha = 3.1 \times 10^{-4}$ and $\beta = 2.8$. Thus the QZ algorithm is typically an order of magnitude faster than either the QR or LR paths.

Clearly, of the three paths tested here for the complex general matrix eigenvalue problem, the QR path (which is also the recommended EISPACK path) yields the most accurate eigenvalues and eigenvectors. However, the QZ path is more economical in computing time and, in view of its satisfactory numerical performance in the NAGLIB implementation, is the preferred path.

VI. Conclusions

This study reported on improvements in the convergence properties of the R algorithm of [10] and investigated the spectral properties of a non-self-adjoint Sturmian eigenvalue equation as the two potentials contained in it, namely V_0 and $\bar{V}$ were varied in a range typical of realistic physical cases. Since the solution procedure of [10] used a Chebyshev series expansion, the present work proposed analytical forms for the potential so that the Chebyshev expansion coefficients could then be generated with high accuracy by recurrence.

In cases where either of the potentials V_0 or $\bar{V}$ had a node inside the range of the other, convergence for eigenvalues was enhanced by a factor of two to five when compared to the case of potentials without nodes. Thus the rate of convergence of the R algorithm was dependent on the choice of the complex potential functions V_0

and $\bar{V}$ or, alternatively, on the spectral properties of the non-self-adjoint differential equation.

The spectral properties of this equation were investigated by continuous variation of the node location for a real potential $\bar{V}$. Cases where the potentials V_0 and $\bar{V}$ were of constant sign had a single branch in the eigenvalue spectrum close to the real axis in an Argand plot. But continuous variation of the node location of $\bar{V}$ leads to the systematic occurrence of eigenvalues far from the origin in the Argand plane. These eigenvalues migrated towards the origin as the node moved to smaller radii and they constituted a second branch in the eigenvalue spectrum. This behaviour is the non-self-adjoint analogue of simpler indefinite self-adjoint eigenvalue problems.

The error in the eigenfunctions was measured by inspection of the L_2 error. In all the cases reported here the L_2 error decreased at least exponentially as a function of N indicating satisfactory convergence behaviour characteristic of a Chebyshev method. For a fixed matrix order a prescribed L_2 error in an eigenfunction is maintained by the nodal potentials for complex eigenvalues of much larger modulus than those of potentials without nodes.

For the complex general matrix eigenvalue problem which results from the method of [10] a comparison was made of the numerical stability of three widely available subroutine paths. The present application found the QR path (EISPACK) to be at most stable and accurate. However, the QZ path (NAGLIB), despite less accuracy, was also stable and more economical in computing time typically by an order of magnitude.

Whereas the previous study [10] demonstrated the viability of the Chebyshev method for solution of a second order non-self-adjoint Sturmian eigenvalue equation, the present work demonstrates advances in numerical performance. This method should be a useful tool in the numerical study of spectral properties of such equations as it complements and extends the limited analyses of (self-adjoint and non-self-adjoint) indefinite Sturm–Liouville problems [18–22]. The method also finds applications in the generation of the basis functions essential to finite rank approximations of the non-self-adjoint integral operators characteristic of Transport and Quantum Scattering theories.

ACKNOWLEDGMENTS

The authors are grateful for the use of computing facilities at the University of the Witwatersrand Computer Centre. They also thank Dr. H. G. Kaper for sending copies of Refs. [19–22] and a referee for suggesting the argument attributed to him in Section III.

REFERENCES

1. L. V. KANTOROVICH AND G. P. AKILOV, *Functional Analysis* (Pergamon, New York, 1982).
2. N. DUNFORD AND J. T. SCHWARTZ, *Linear Operators, Parts I, II* (Wiley–Interscience, New York, 1963).

3. R. G. NEWTON, *Scattering Theory of Waves and Particles* (Springer-Verlag, New York, 1982).
4. H. G. KAPER, C. G. LEKKERKERKER, AND J. HEJTMANEK, *Spectral Methods in Linear Transport Theory* (Birkhaeuser-Verlag, Basel, 1982).
5. P. G. DRAZIN AND W. H. REID, *Hydrodynamic Stability* (Cambridge Univ. Press, London, 1982).
6. N. DUNFORD AND J. T. SCHWARTZ, *Linear Operators, Part III* (Wiley–Interscience, New York, 1971).
7. E. MUELLER-PFEIFFER, *Spectral Theory of Ordinary Differential Operators* (Ellis Horwood Ltd., Chichester, 1981).
8. I. C. GOHBERG AND M. G. KREIN, *Introduction to the Theory of Linear Nonselfadjoint Operators* (Amer. Math. Soc., Providence, R.I., 1969).
9. J. R. RINGROSE, *Compact Non-Self-Adjoint Operators* (Van Nostrand–Reinhold, New York, 1971).
10. G. DELIC AND G. H. RAWITSCHER, *J. Comput. Phys.* **57**, 188 (1985).
11. G. H. RAWITSCHER AND G. DELIC, *Phys. Rev. C* **29**, 1153 (1984).
12. R. Y. RASOANAIVO, Ph.D. thesis, University of Connecticut, 1982.
13. J. M. VARAH, *J. Comput. Phys.* **54**, 87 (1984).
14. G. H. RAWITSCHER AND G. DELIC, *J. Math. Phys.* **27**, 816 (1986).
15. M. A. BREBNER AND J. GRAD, *Linear Algebra Appl.* **43**, 99 (1982).
16. C. R. CRAWFORD, *Comm. ACM* **16**, 41 (1973).
17. Y. L. LUKE, *The Special Functions and Their Approximations*, Vols. I, II (Academic Press, New York, 1969).
18. A. B. MINGARELLI, in *Proceedings, Seventh Conference on Ordinary and Partial Differential Equations, Dundee, Scotland, 1982*, edited by W. N. Everitt and B. D. Sleeman (Springer-Verlag, Berlin, 1982), p. 519.
19. *Proceedings, 1984 Workshop on Spectral Theory of Sturm–Liouville Differential Operators*, Argonne National Laboratory, U.S.A., May 14–June 15, 1984, edited by Hans G. Kaper and Anton Zettl (ANL-84-73).
20. H. G. KAPER, M. K. KWONG, AND A. ZETTL, *Monatsh. Math.* **97**, 177 (1984).
21. H. G. KAPER, M. K. KWONG, C. G. LEKKERKERKER, AND A. ZETTL, *Proc. R. Soc. Edinburgh Ser. A* **98**, 69 (1984).
22. H. G. KAPER, M. K. KWONG, C. G. LEKKERKERKER, AND A. ZETTL, Argonne National Laboratory Report Number ANL-83-76, 1983. preprint ANL-83-76.
23. G. DELIC, in preparation.
24. B. T. SMITH, J. M. BOYLE, J. J. DONGARRA, B. S. GARBOW, Y. IKEBE, V. C. KLEMA, AND C. B. MOLER, *Matrix Eigensystem Routines—EISPACK Guide*, Lecture Notes in Computer Science, G. Goos and J. Hartmanis, eds. (Springer-Verlag, Berlin, 1976).
25. C. B. MOLER AND G. W. STEWART, *SIAM J. Numer. Anal.* **10**, 241 (1973).
26. *International Mathematical and Statistics Library Reference Manual* (Ed. 9.1) (International Mathematical and Statistics Library, Houston, 1983).
27. *Numerical Algorithms Group Library Manual (Mark 11)*, (Numerical Algorithms Group, Oxford, 1984).